Journal of Alloys and Compounds 513 (2012) 35–43

Contents lists available at SciVerse ScienceDirect

Journal of Alloys and Compounds

journal homepage: www.elsevier.com/locate/jallcom

A study on the optical, structural, electrical conductivity and dielectric properties of a lithium bismuth germanium tungsten glasses

Shaaban M. Salem[a,*], E.K. Abdel-Khalek[a,c], E.A. Mohamed[b,c], M. Farouk[a,c]

[a] Department of Physics, Faculty of Science, Al Azhar University, Nasr City 11884, Cairo, Egypt
[b] Department of Physics, Faculty of Science (Girl's Branch), Al Azhar University, Nasr City, Cairo, Egypt
[c] Department of Physics, Faculty of Science, Jazan University, Saudi Arabia

ARTICLE INFO

Article history:
Received 17 January 2011
Received in revised form
18 September 2011
Accepted 19 September 2011
Available online 18 October 2011

Keywords:
Lithium–tungsten–bismuth–germanium glasses
Optical, structure, electrical conductivity and dielectric properties

ABSTRACT

Glasses in the system $(65-x)Bi_2O_3$–$15Li_2O$–$20GeO_2$–xWO_3 (where $x = 2$, 5 and 10 mol%) were prepared by normal melt quenching method. The change in density and molar volume in these glasses indicates the effect of WO_3 on the glass structure. Fourier transform infrared (FT-IR) spectra show that these glasses are made up of GeO_4, GeO_6, BiO_6, BiO_3, WO_4 and WO_6 basic structural units. The structural units of BiO_6, GeO_6 and WO_6 increase with the increasing of WO_3 content. The optical constants of these glasses are determined over a spectral range, providing the complex dielectric constant to be calculated. Higher values for the refractive index and dispersion are recorded due to the high polarizability of bismuth and tungsten ions. The values of the optical band gap E_g for all types of electronic transitions and refractive index have been determined and discussed. The dc conductivity measured in the temperature range 423–623 K obeys Arrhenius law. The dielectric constant (ε'), dielectric loss ($\tan\delta$) and ac conductivity over a wide range of frequency and temperature, of the glasses were investigated.

1. Introduction

Recently, glasses containing tungsten ions have many technological applications owing to their important optical and electrical properties [1–3]. Such properties depend mainly on the existence of tungsten ions in various oxidation states (hexavalent W^{6+}, pentavalent W^{5+} and also in tetravalent W^{4+} state) regardless of the oxidation state of the tungsten ion in the starting glass batch [4]. The tungsten W^{6+} ions participate in the glass network with different structural units like WO_4 (T_d) and WO_6 (O_h) structural units and W^{5+} ions participate in the form of $W^{5+}O_3^-$ and occupy octahedral positions [5]. Thus the presence of tungsten ions in different structural groups and oxidation states in the glass matrix at a given temperature depends on the quantitative properties of modifiers, glass formers, mobility of the modifier cation, etc. [6–8]. On the other hand, glasses containing two glass-forming oxides, such as the bismuth germanate glasses, which have superior properties, have a wide range of practical applications [7–9]. These glasses are attractive to researchers because of their unique structural characteristics, which result from coordination changes in bismuth and germanium. GeO_2 is a typical glass former while Bi_2O_3 are conditional glass former [10,11]. GeO_2 alone can form a glass network that consists of tetrahedra and octahedra of germanium coordinated by oxygen [12]. Despite the fact that Bi_2O_3 is not a classical glass network former, due to its high polarizability, in the presence of conventional glass-forming cations such as P^{5+}, Si^{4+}, B^{3+}, it may build a glass network of both BiO_6 octahedral and BiO_3 pyramidal units [13]. In view of the aforementioned aspects $(65-x)Bi_2O_3$–$15Li_2O$–$20GeO_2$–xWO_3 (where $x = 2$, 5 and 10 mol%) glasses have been synthesized. The aim of the present work has been carried out to investigate the effect of replacement of Bi_2O_3 by WO_3 on the density, molar volume, structural, electrical conductivity, optical and dielectric properties of glasses.

2. Experimental

Glass samples of $(65-x)Bi_2O_3$–$15Li_2O$–$20GeO_2$–xWO_3 (where $x = 2$, 5 and 10 mol%) were prepared by normal melt quenching technique. The glass samples under investigation were prepared from Analar grade reagents of WO_3, GeO_2, Bi_2O_3 and lithium carbonate. The batches were melted in a porcelain crucibles at 1100 °C for about 45 min until a bubble free liquid was formed. The resultant melt was then cast in a brass mould and subsequently annealed at 300 °C. The density d of glasses was determined by the standard principle of Archimedes' using carbon tetrachloride ($\rho = 1.53$ kg/m^3) as an immersion liquid. The molar volume (V_m) was calculated using the relation $V_m = M_T/d$ where M_T is the total molecular weight of the multicomponent samples. The glasses were then ground and optically polished. Infrared spectra of the powdered glass samples were recorded at room temperature in the range 320–1230 cm^{-1} using a spectrometer (Perkin-Elmer FT-IS, model 1605). These measurements were made on glass powder dispersed in KBr pellets. The UV transmittance and reflectance spectra were recorded in the range of 190–1100 nm Jasco V-570 Spectrophotometer. For the DC conductivity, the bulk samples were highly polished; the two surfaces of each pellet were coated with silver paste. The DC

* Corresponding author. Tel.: +20 238952044.
E-mail address: shaabansalem@gmail.com (S.M. Salem).

0925-8388/$ – see front matter © 2011 Elsevier B.V. All rights reserved.
doi:10.1016/j.jallcom.2011.09.052

Table 1
Physical properties for the studied glass system.

X mol%	d (g/cm^3)	V_m (cm^3/mol)	$N \times 10^{22}$ (cm^3)	R (A)	r_p (A)
2	6.35	51.99	1.65	3.93	1.58
5	6.12	52.81	1.59	3.98	1.60
10	5.88	52.97	1.53	4.03	1.62

conductivity measured by means of two-probe method, which is appropriate for high resistance materials. The current is monitored by means of a Picometer with heating rate 2 K/min, constant voltage source 18.9 V and a home-made furnace. The dielectric constant ε, AC conductivity and dielectric loss tangent ($\tan\delta$) of the samples were measured in the temperature range 300–650 K, and frequency range of (0.12–100 kHz) using a bridge system (Stanford model SR 720 LCR meter).

3. Results and discussion

3.1. Density and molar volume

The density, molar volume, concentration of tungsten ions N, the mean spacing between tungsten ions R and the polaron radius r_p (where N, R and r_p are calculated using the relations reported earlier [14]) for glass samples as a function of WO_3 content are listed in Table 1. From this table it can be seen that the density of samples decreases while the molar volume increase with increasing of the WO_3 content. This can be attributed to several reasons, firstly the molecular weight of WO_3 is lower than the molecular weight Bi_2O_3. Thus decrease of a heavy metal ion leads to a decrease in the density that has dependence on the composition. Secondly the transformation of some tungsten, bismuth and germanium from the fourfold coordination to sixfold coordination states. Also this result is due to the fact that tungsten ions have an intermediate behavior between network formers and modifiers. Thus, depending on the own nature of the other glass components in the three-dimensional structure and on their percentage, they could play the role of formers or modifiers and introduces excess structural free volume [15].

3.2. FT-IR spectra

Fig. 1 shows the FT-IR absorption spectra for glass samples containing 2, 5 and 10 mol% WO_3 in the wavenumber range 320–1230 cm^{-1}. The infrared spectrum of glass sample containing 2 mol% WO_3 showed the presence of broad bands at 371, 410, 472, 510, 709, 745, 1015 and 1103 cm^{-1}. Shoulders around 600, 844 and 935 cm^{-1} were also observed. The broadening of bands is due to the disorderness. The band around 371 cm^{-1} is due to the bending vibrations of W–O–W in the WO_6 units [16]. The three bands appeared at 410, 472, and 510 cm^{-1} are assigned to the Bi–O bending vibrations in BiO_6 units [15] and the band around 472 cm^{-1} may be ascribed to bending vibrations of the bonds (Bi–O–W) [14]. The shoulder around 600 cm^{-1} is assigned to the stretching vibration in the BiO_6 units [17]. The band at 709 cm^{-1} is assigned to Ge–O–Ge stretching vibration in GeO_6 units while the band at 745 cm^{-1} identified as due to Ge–O bonds vibrations in GeO_4 units [18–20]. The shoulder at 935 cm^{-1} and the weak shoulder at 844 cm^{-1} corresponding to the vibration of WO_3 (υs of WO_4 and υas of WO_6, respectively) [15]. The band at 1015 cm^{-1} is assigned to the Ge–O stretching vibrations in GeO_4 units [21]. The band at about 1103 cm^{-1} can be due to the Bi–O–Bi or Bi–O–Ge linkage vibrations [22]. Infrared absorption band was observed at 1103 cm^{-1} in the present glass samples, and it was attributed to the linkage vibration of Bi–O–Ge or Bi–O–Bi. With the WO_3 content increases, these bands shifted to higher wavenumber, thus indicating that WO_3 caused changes in the glass network. This represents the substitution of BiO_6 octahedral by WO_4 tetrahedra. The Bi–O–W linkages are expected to form from the Bi–O–Bi and W–O–W species, because both bismuth and tungsten ions have comparable electronegativity values (2.02 and 2, respectively) and can therefore substitute for each other in bonding with oxygen atoms. Although, it can be seen from Fig. 1 the intensity of the bands at 472 and 745 cm^{-1} decreases while the broadening of this band increase. These bands correspond to the Bi–O bending vibrations in BiO_6 units and Ge–O bonds vibrations in GeO_4 units in the glass, respectively. This result can be associated to changes in the coordination of Ge atoms, from four to six, in the glass samples [23]. It is clear from Fig. 1 that the relative intensity of the shoulder band 935 cm^{-1} decreases with respect to the prominent band at 371 cm^{-1} as WO_3 content increases. This result indicates that the W ion coordination state changes from fourfold coordination WO_4 to sixfold coordination WO_6. On the other hand, there is increase in the relative intensity and broadening of the two bands around 1015 and 1103 cm^{-1}, which ascribed to stretching vibrations in GeO_4 and the linkage vibration of Bi–O–Ge and/or Bi–O–Bi units, respectively, with increase WO_3 content in the glass matrix, which can be due to the contribution of the vibrations of W–O bonds of WO_6 units.

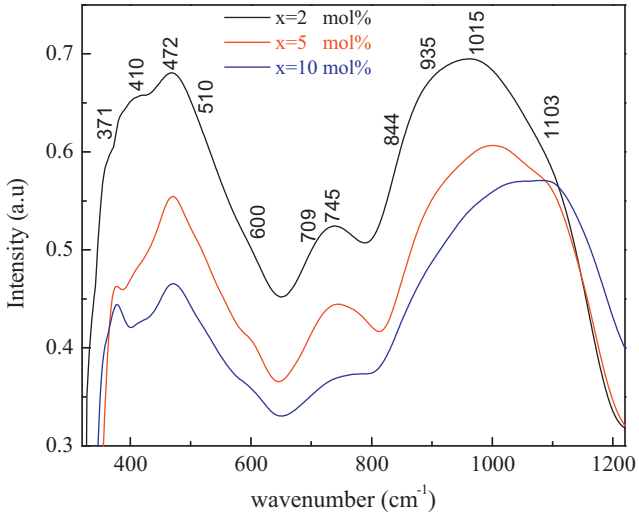

Fig. 1. FT-IR absorption spectra of $(15Li_2O–(65-x)Bi_2O_3–20GeO_2–xWO_3$ where x = 2, 5 and 10 mol%) the wavenumber region 320–1230 cm^{-1}.

3.3. Optical properties

Fig. 2 shows the UV transmittance and reflectance spectra for glass samples containing 2, 5 and 10 mol% WO_3 in the wavelength range 190–1100 nm. From this figure it is found that the visible transmittance of the samples decreases and the positions of the λ_c shift towards red when tungsten increases. This shift to higher wavelength can be attributed to the increase in the non-bridging oxygen, which in turn gives rise to a decrease in bridging oxygen. Since non-bridging oxygen are bonded to only one framework cation and bridging oxygen are bonded to two network cations. The UV transmittance and reflectance spectra of present glass system exhibit a weak band in the region 800–1000 nm reveal the presence of W^{5+} in addition to W^{6+} ions. This broad visible band is assumed to be due to the excitation of the W^{5+} ion from $b_2(xy)$ ground state with crystal field parameters around Δ = 16,000 cm^{-1} and δ = 13,000 cm^{-1} [24]. Two optical excitations were predicted starting from this ground state, but because of the strong intervalence charge transfer transition between W^{5+} and W^{6+} ions, the two bands could not be resolved in the spectra of studied glasses [5]. They further assumed that the lower intensity and half width of the identified band observed suggested that the concentration

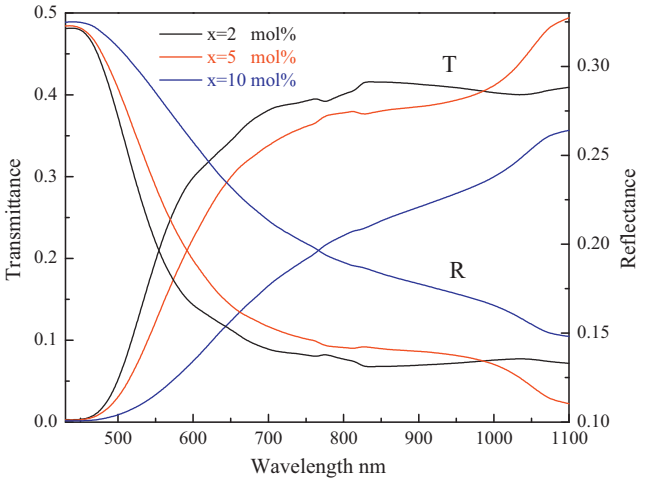

Fig. 2. The transmittance and reflectance spectra for the studied glasses.

of W^{5+} ions in this system is relatively low. According to Lambert's absorption law, the absorption coefficient as a function of attenuation factor, η, and the thickness of the glass sample, t, is defined as:

$$\eta(\lambda) = \exp[-\alpha(\lambda)t] \quad (1)$$

A way of data reduction based on an iteration method is used to calculate η and the optical constants n and k from the overall reflectance $R(\lambda)$ and transmittance $T(\lambda)$ of the glass samples. The optical absorption coefficient, α, which is the relative rate of decrease in light intensity along its path of propagation, Fig. 3 shows a plot of α as a function of wavelength for the glass system. The optical absorption coefficient α of the studied glasses can be evaluated from the optical transmittance, reflectance, and the thickness of the sample t as:

$$\alpha = \left[\frac{1}{t}\right] \ln\left[\frac{(1-R)}{T}\right] \quad (2)$$

The UV-absorption edges of the studied glass are not sharply defined which characterizes the glassy nature of samples. The absorption coefficient α as a function of the photon energy ($h\upsilon$)

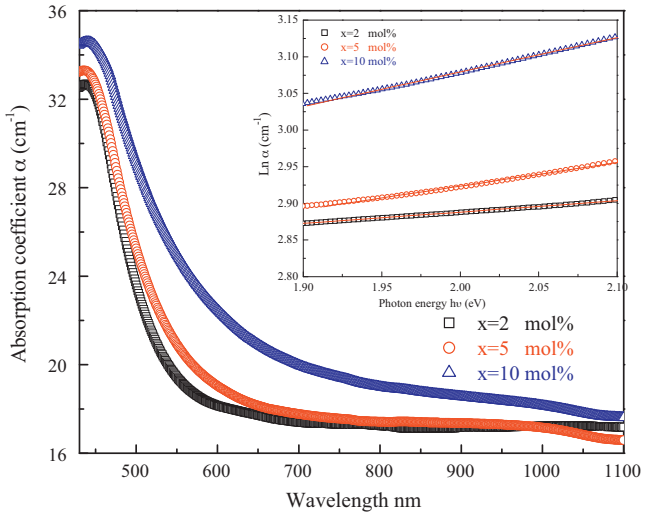

Fig. 3. The absorption coefficient α as a function of wavelength and inset, the relation between $\ln\alpha$ cm^{-1} and photon energy eV for the studied glasses.

for direct and indirect optical transitions, according to Pankove is given by [25]:

$$(\alpha(\upsilon)h\upsilon)^p = A(h\upsilon - E_g) \quad (3)$$

The exponent p determines the type of electronic transitions causing the absorption and takes the values 1/2, 2/3, 2 and 1/3 for indirect allowed, direct forbidden, direct allowed and indirect forbidden transitions, respectively, and A is a constant related to the extent of the band tailing [26]. The values of optical band-gap energy E_g can be obtained by extrapolating the absorption coefficient to zero absorption in the $(\alpha h\upsilon)^p$ against photon energy $h\upsilon$ plot as shown in Fig. 4. The energy of the optical band gap was evaluated for the glass samples at different values of P and listed in Table 2. As seen in Table 2 the obtained values of the optical gap are changing according to the selected value of the exponent P. Moreover, the change in the value of the regression factor does not really decide which value of P is better to be selected. Therefore, Eq. (4) may be rather used only for the determination of the type of conduction mechanism, and E_g itself should be determined using another parameter the imaginary part of the dielectric constant, ε_2 by which the exact value of exponent can be selected. The value of optical band gap is observed decreasing with the increase of WO_3 for any value of P. Urbach and optical band gap energy could be explained in terms of the structure of the prepared glasses. Tungsten ions may be inserted in the bismuth–germanium–tungsten chains that lead to a more ordered glass matrix. Therefore, the introducing of WO_3, which acts as network intermediate modifier to the glasses, increases the connectivity of the network and hence Urbach energy and optical energy gap in present glasses are smaller than the values of Urbach and optical energy for anther glasses. On the contrary, Urbach energy increase and the optical energy gap decreases with increasing WO_3 concentration.

The values of refractive index were estimated $n = (1+R^{1/2})/(1-R^{1/2})$, R is reflectivity of the sample in the transparent region of glasses studied [17]. Fig. 5(a) and (b) shows the extinction coefficient, and refractive index as a function of wavelength for the glass system, the extinction coefficient is the imaginary part of the complex index of refraction, which also relates to light absorption. It is clear that, the refractive index n as shown in Fig. 5(b) decreases with increasing the wavelength of the incident photon, and on the contrary increases with the increase in the WO_3 content. Thus, the dependence of the refractive indices on the WO_3 content of the studied glasses can be explained as follows. According to the Lorentz–Lorenz [27] equation, there are some factors influences the increase of the refractive index such as, the coordination number, Z, of the studied glasses. Introducing WO_3 causes as discussed previously, the increase in the coordination number of the glasses [28]. Also, the creation of NBOs creates more ionic bonds which manifest themselves in a larger polarizability over the mostly covalent bonds of bridging oxygen providing a higher index value. The complex dielectric function describes the interaction of electromagnetic waves with matter. It reflects by that interaction the underlying molecular mechanism [29]. The complex dielectric, ε, constant components of a material in terms of the optical constants n and k are given as:

$$\varepsilon_1 = n^2 - k^2 \quad \text{and} \quad \varepsilon_2 = 2nk \quad (4)$$

where ε_1 and ε_2 are the real and imaginary part, respectively. Fig. 6(a) shows the real part of the dielectric constant, ε_1, versus the photon energy $h\upsilon$ for the present glass samples. For all samples the dielectric constant shows an exponential steady increase with photon energy and with the increase of the concentration of WO_3. This means that the free carrier concentration of the different glass compositions change in the same way with the change in WO_3 content, which is consistent with the increase of the glass index of refraction with increasing WO_3. Fig. 6(b) shows the imaginary part

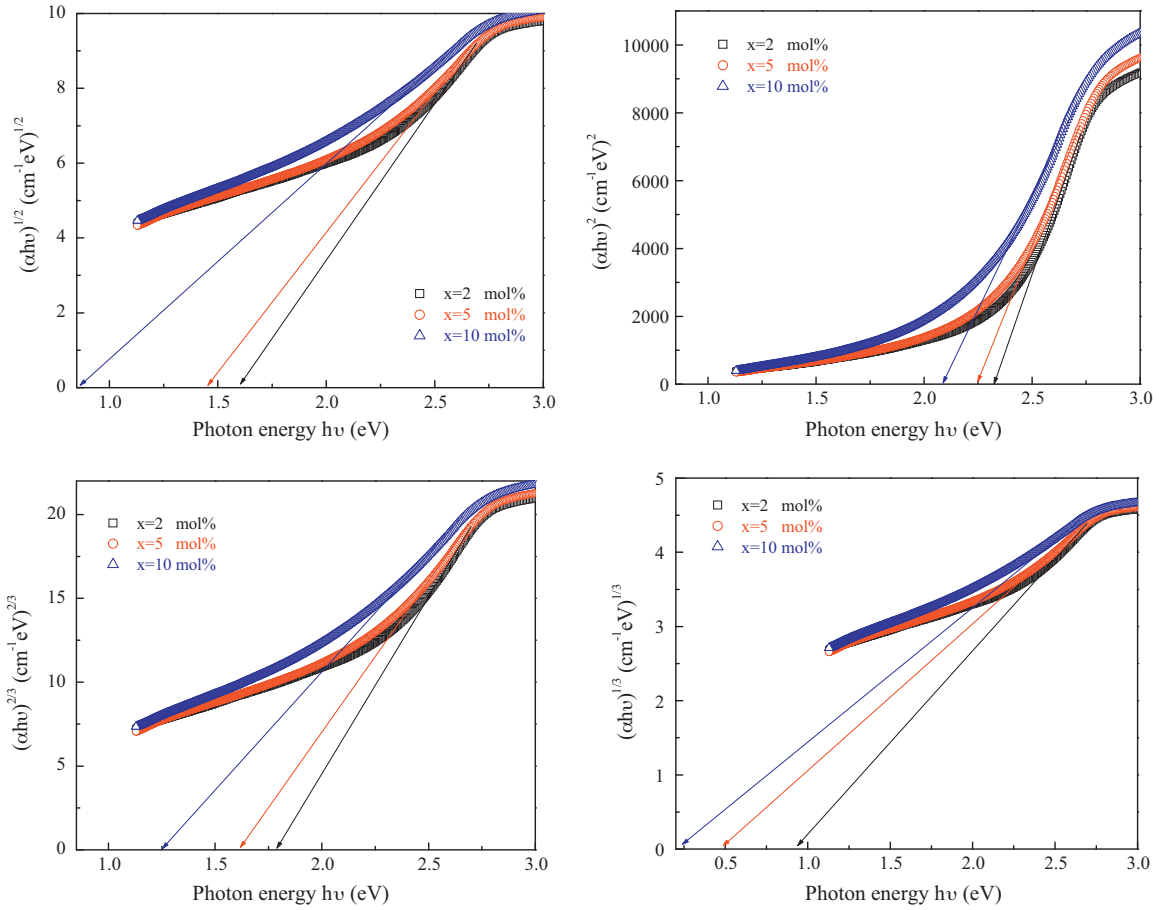

Fig. 4. The relation between $(\alpha h\upsilon)^p$ against photon energy $h\upsilon$ where $p = 1/2$, 2/3, 2, and 1/3 for the glass system.

of the dielectric constant, ε_2, versus the photon energy for the studied glass system, the fundamental absorption band which could be determined from the measurements of reflectivity at normal incidence [26]. The absorption band is obtained when the imaginary part of the dielectric constant is plotted as a function of photon energy. The behavior of ε_2 and n suggests that hole exchanges are in the local displacements of electrons or holes in the direction of the electric field, which then cause polarization. On a comparison of the optical energy gap values obtained from the transmittance and reflectance spectra in the case of indirect allowed transition are in good agreement with the values estimated from the dielectric measurements ε_2, however, the type of electronic transitions in the present glass system is indirect allowed. The refractive index variation with respect to photon energy could be obtained from the following relationship, based on the single oscillator approximation suggested by Wample [30]:

$$n^2 - 1 = \frac{E_d E_o}{[E_o^2 - E^2]} \tag{5}$$

where n is the refractive indices at a specific wavelength, $E = h\upsilon$ is the photon energy, E_o is the average electronic energy gap for transition and E_d is the electronic oscillator strength. E_o and E_d can be determined from the linear fit of $1/(n^2 - 1)$ versus E^2 (see Fig. 7). The values of E_o and E_d were listed in Table 2. It is clearly seen from this table that the average electronic energy gap E_o decreases as WO_3 increase. The lack of crystalline long-range order in amorphous or glassy materials is associated with a tailing of density of states [31]. At lower values of the absorption coefficient, the extent of the exponential tail of the absorption edge characterized by the Urbach energy and it is given by:

$$\alpha(h\upsilon) = \alpha_o \exp\left(\frac{h\upsilon}{E_r}\right) \tag{6}$$

where α_o is a constant, E_r is the Urbach energy which indicates the width of the band tails of the localized states. The optical absorption coefficient just below the absorption edge shows exponential variation with photon energy indicating the presence of Urbach's tail. From the curves of $\ln(\alpha)$, against photon energy, $h\upsilon$, the Urbach energy is calculated for the glass taking the reciprocals of the slopes of the linear portion in the lower photon energy of these curves, see inset of Fig. 3. The values of E_r for different compositions are listed in Table 2. The exponential dependence of the optical absorption coefficient with photon energy may arise from the electronic transitions between the localized states, which have tailed odd in the

Table 2
Optical energy gap values E_g obtained for different types of transitions and E_g from ε_2, E_r, average oscillator energy for electrons E_o, dispersion energy parameter E_d, respectively, for the studied glasses.

X mol%	$p = 1/2$	$p = 2$	$p = 2/3$	$p = 1/3$	$E_g - \varepsilon_2$	E_r	E_o	E_d	α_m (A)	M
2	1.61	2.31	1.78	0.93	1.75	0.045	2.85	6.06	41.41	0.45
5	1.44	2.24	1.61	0.48	1.53	0.047	2.82	7.23	43.18	0.43
10	0.86	2.08	1.24	0.21	0.85	0.067	2.80	10.79	49.47	0.35

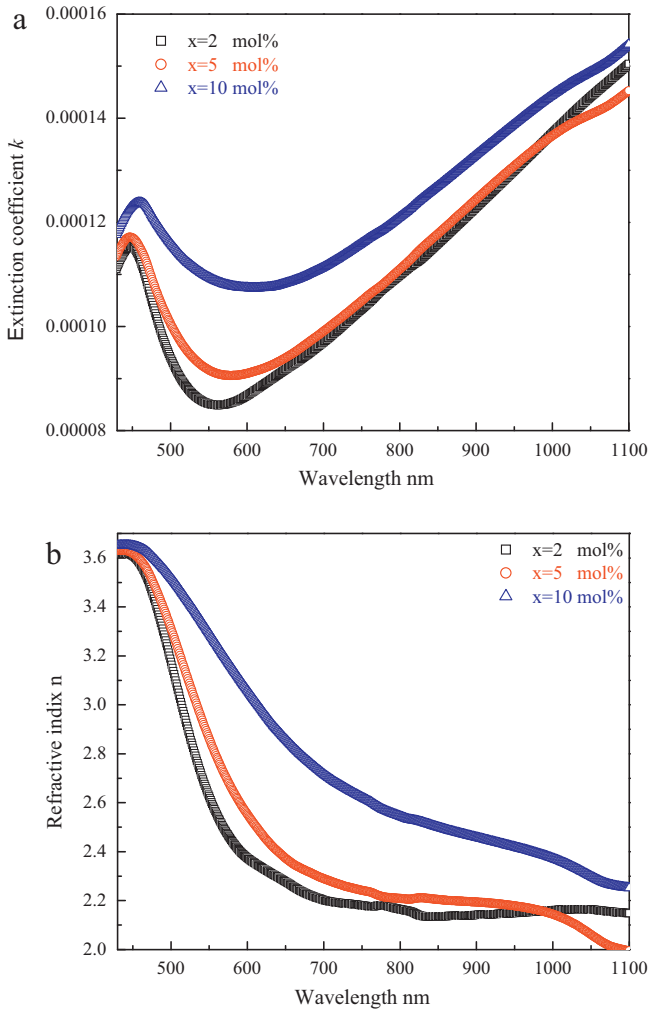

Fig. 5. (a) The extinction coefficient k, and (b) refractive index n as a function of wavelength for the glass system.

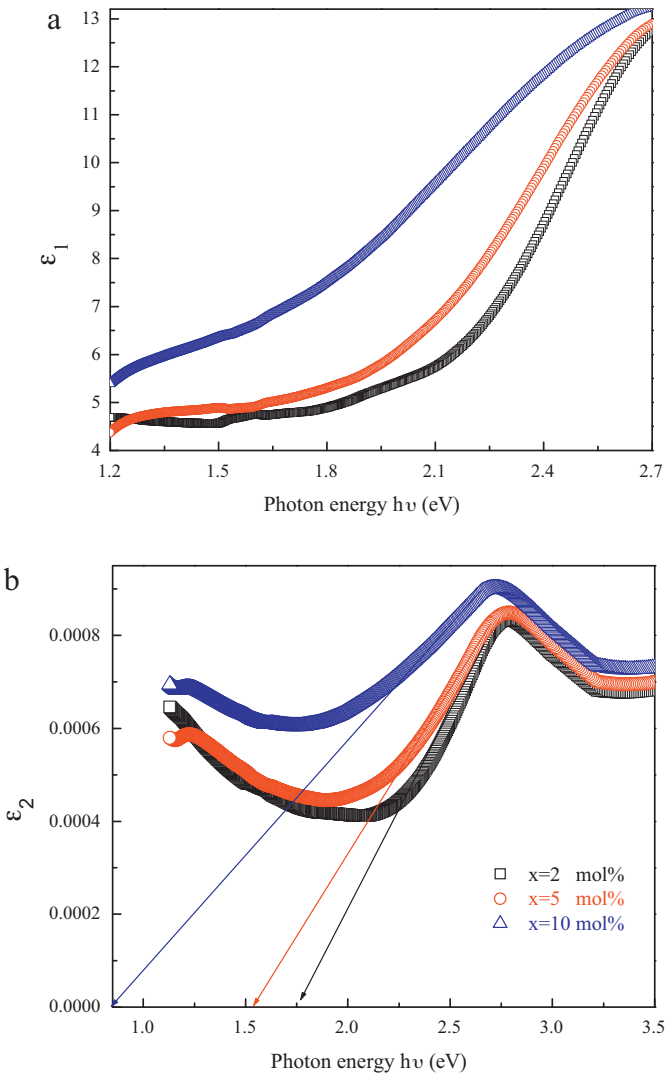

Fig. 6. (a) The real and (b) imaginary part of the dielectric constant is plotted as a function of photon energy for the glass system.

band gap. The density of these states falls off exponentially with energy, which is consistent with the theory of Tauc [31]. However, the exponential dependence of the optical absorption coefficient on energy might arise from the random fluctuations of the internal fields associated with the structural disorder in many materials. The values of E_r and E_g for indirect allowed transition as shown in Table 2, the E_g decreases while E_r increases with an increase in WO_3 content. The behavior of E_r and E_g versus WO_3 content can be attributed to the structural changes that are taking place in the studied glass system. According to the FT-IR analysis, germanium and bismuth have more than one stable configuration [32,33]. The relation between the refractive indices, molar volume and the molar refraction R_m is given by [34]:

$$R_m = \frac{[(n^2-1)/(n^2+2)]}{V_m} \tag{7}$$

where $R=(n^2-1)/(n^2+2)$ is known as the reflection loss and n is the refractive index. The molar refraction is proportional to the molar electronic polarizability of the material, α_m, according to the relation $\alpha_m=(3/4\pi N)R_m$, where N is the number of polarizable ions per mole [34]. The increase in molar refraction and the increase in refractive index accompany the increase in polarizability. According to the theory on metallization of the condensed matter proposed by Herzfeld, the necessary conditions for predicting the non-metallic nature of the solid are: $R_m/V_m > 1$ (metal) and $R_m/V_m < 1$ (non-metal) [35]. The difference from unity

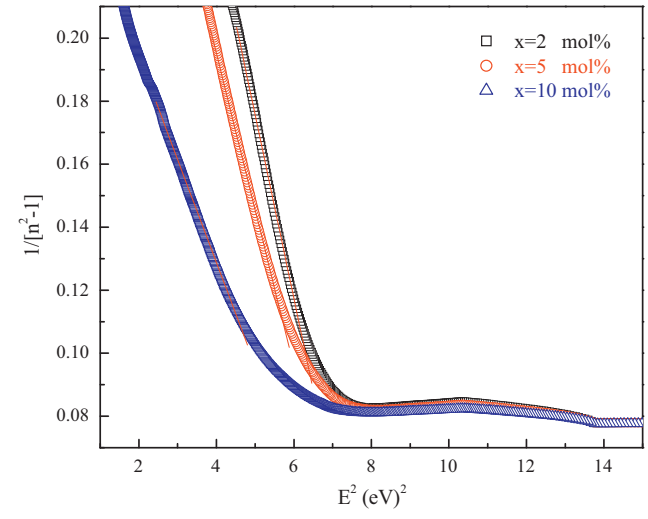

Fig. 7. The relation between $1/(n^2-1)$ and E^2 for the glass system.

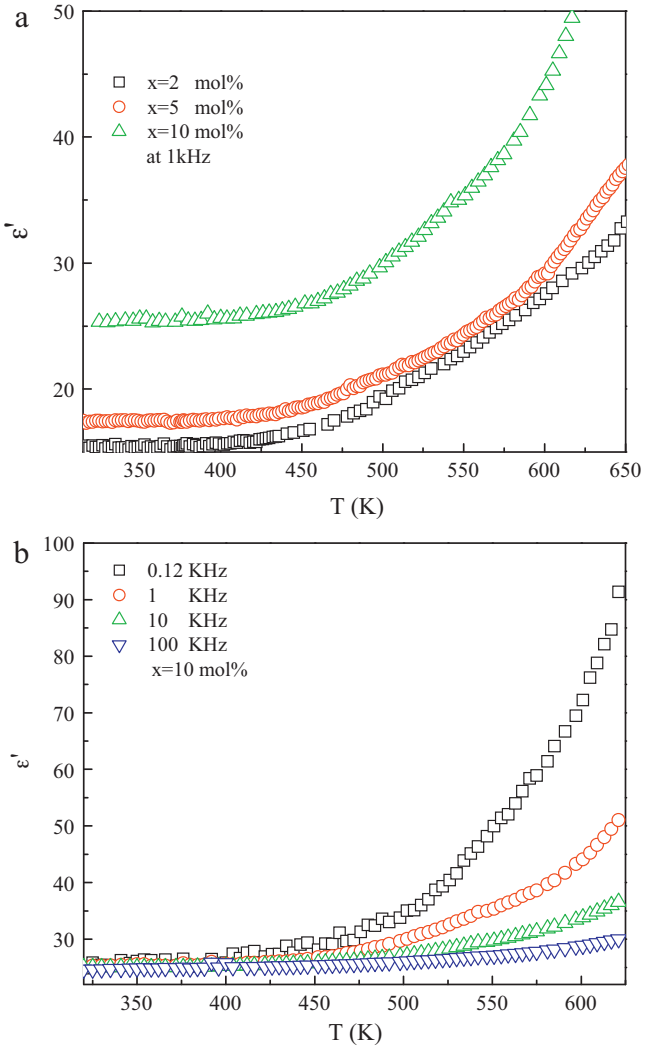

Fig. 8. (a) A comparison plot of variation of dielectric constant with temperature at 1 kHz for the studied glasses. (b) Variation of dielectric constant with temperature at different frequencies for $x = 10$ mol%.

$M = 1 - (R_m/V_m)$ is called metallization criterion [36]. The obtained values of α_m, and M are listed in Table 2.

3.4. Dielectric properties

The variation of the dielectric constant as a function of temperature at 1 kHz for the glass samples containing 2, 5 and 10 mol% WO_3 are depicted in Fig. 8(a). From this figure it can been that the dielectric constant ε' increases with increase of temperatures and WO_3 content. The variation of the dielectric constant as a function of temperature at various frequencies (120 Hz to 100 kHz) for the sample containing 10 mol% WO_3 is shown in Fig. 8(b). The dielectric constant (Fig. 8(b)) becomes larger at lower frequencies and at higher temperatures which is normal in oxide glasses and is not an indication for spontaneous polarization [37,38]. This may be due to the fact that as the frequency increases, the polarizability part from ionic and orientation sources decreases and finally vanishes due to the inertia of the ions. At low temperatures, the contribution of electronic and ionic components to the total polarizability will be small. As the temperature is increased the electronic and ionic polarizabilities sources start to increase [38,39].

The variation of the dielectric loss ($\tan\delta$) as a function of temperature at various frequencies (120 Hz to 100 kHz) for the sample containing 10 mol% WO_3 is shown in Fig. 9. The value of $\tan\delta$ is found to increase with increase in temperature especially at higher temperatures and at lower frequencies. It should be noted from this figure that $\tan\delta$ at low frequency increases, where dc conductivity dominates. The frequency dependence of $\tan\delta$ is associated with losses by conduction or movement of charge carriers throughout the glass network, creating conduction losses. Consequently, dielectric losses for samples with higher electrical conductivity are higher than for the samples having low electrical conductivity. The increase in dielectric constant (ε') values with increasing WO_3 content could be attributed to charge transfer transition between W^{5+} and W^{6+} ions. Such tendency suggests that tungsten ions occupy octahedral positions, crosslink decrease with the other structural units and decrease the rigidity of the glass network. In other words such cross-linkages decrease the concentration of free charge carriers that would build up space charge polarization.

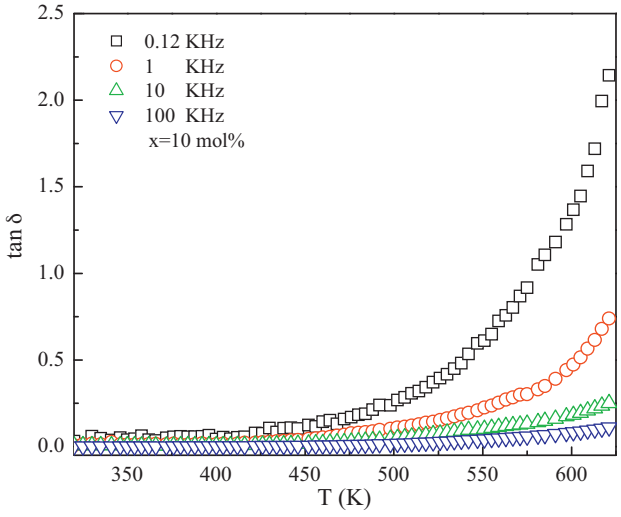

Fig. 9. Variation of dielectric loss $\tan\delta$ with temperature at different frequencies for sample $x = 10$ mol%.

3.5. Electrical conductivity

The understanding of the conductivity is often used to conclude information regarding the dynamic behavior of ion conducting materials. The low frequency spectra of conductivity are frequency independent and are illustrated as dc conductivity. The temperature dependence of the dc conductivity gives information about the long time ion dynamics and it is well described by the Arrhenius law, reflecting the activated nature of ionic hopping processes. At high frequencies, the conductivity becomes strongly frequency dependent, varying approximately as a fractional power of frequency. The frequency dependent electrical conductivity σ_{ac} increases approximately linearly with angular frequency ω up to 108 Hz [40]:

$$\sigma = \sigma_{ac} + \sigma_{dc} = A\omega^s + \sigma_{dc} \quad (8)$$

where σ_{dc} is the frequency-independent component, A is a temperature dependent constant, s is the frequency exponent and $\sigma_{ac} = A\omega^s$ represents ac or dissipative contribution to the total conductivity, which depends on frequency, temperature and composition of the sample.

3.5.1. DC conductivity, σ_{dc}

The reciprocal temperature dependence of the DC conductivity, σ_{dc}, for glass samples containing 2, 5 and 10 mol% WO_3 are shown in Fig. 10. From this figure it can be seen that σ_{dc} increases with

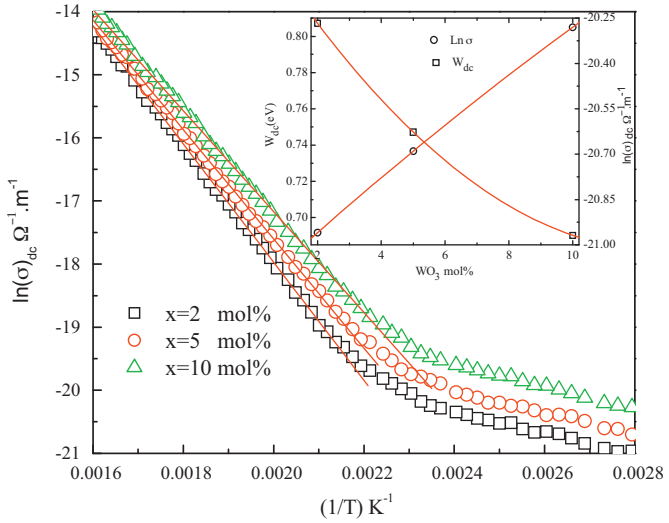

Fig. 10. A comparison plot of variation of ($\ln \sigma_{dc}$) with ($1/T$) for the studied glasses. Inset variation of ($\ln \sigma_{dc}$) and W_{dc} as function of composition.

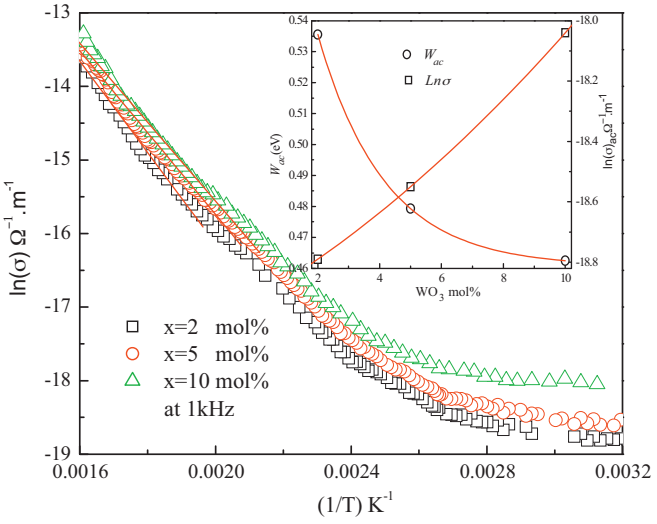

Fig. 11. A comparison plot of variation of $\ln(\sigma)$ with $1/T$ measured at 1 kHz for the studied glasses. Inset variation of $\ln(\sigma)$ and activation energy W as function of composition.

increase in temperature, indicating the semiconducting nature of the present glasses within the studied range of temperature (320–762 K). The variation of σ_{dc} was also observed to be a thermally activated process and is due to the hopping of polarons between the multivalent states of transition metal ions in the glass matrix [41]. The temperature dependence of both pure DC and AC conductivities has been considered in the light of Mott's small polaron hopping model. The electrical conductivity in the non-adiabatic regime is expressed as [42]:

$$\sigma = \left(\frac{\sigma_o}{T}\right) \exp\left(\frac{-W}{KT}\right) \quad (9)$$

where W is the activation energy and σ_0 is the pre-exponential factor, k is the Boltzmann constant and T is absolute temperature. This is likely to facilitate greater mobility of ions resulted an increase in conductivity and decreases the activation energy. The average distance R between tungsten ions is calculated as $R = (1/N)^{1/3}$ where N is the concentration of tungsten ions per unit volume (Table 1). Using the values R, the polaron radius r_p is estimated as $r_p = R/2(\pi/6)^{1/3}$ for a non-dispersive system. The possible effect of disorder has been neglected in the above calculation; the small values of polaron radii suggest that the polarons are highly localized [43]. Inset of Fig. 10 shows the plot of activation energy, W and electrical conductivity at fixed temperature 325 K, as a function of WO_3 content. It is observed that as the WO_3 content increase the activation energy of conduction decreases. Such a behavior is characteristic of SPH in this system [42]. From Inset of Fig. 10 it can be seen that the conductivity increases with increase in WO_3 concentration such behavior is likely to arise due to the structural changes occurring in glass network. In the present glass system, the effective of modifier concentration Li_2O and WO_3 leads to the reconversion of the structural units of BiO_3, GeO_4 to BiO_6, GeO_6 units. Due to the creation of non-bridging oxygen, the openness of the net work results in the weakening of the structure.

3.5.2. AC conductivity, σ_{ac}

The reciprocal temperature dependence of the total conductivity σ, at 1 kHz for glass samples containing 2, 5 and 10 mol% WO_3 are shown in Fig. 11. The reciprocal temperature dependence of the total conductivity σ as a function of frequency (120 Hz to 100 kHz) for the sample containing 10 mol% WO_3 is shown in Fig. 12. The values of AC activation energies W obtained for the samples from the slope of $\ln \sigma(\omega)$ versus ($1/T$). The increase of applied field frequency enhances the electronic jumps between localized states, and consequently, the activation energy W decreases, which confirms the hopping conduction between the defect centres around Fermi level to be a dominant mechanism of conduction. This means that $\sigma(\omega)$ at high frequencies is not thermally activated in a relatively wide range of temperatures. On the other hand, at lower frequencies and higher temperatures, the AC conductivity is temperature dependent, similar to that of DC conductivity. The activation energy is found to decrease while the conductivity increases with increase in WO_3 content as shown inset of Fig. 11. Because, the conductivity is associated with increase in the concentration of mobile electrons or polarons, indicating an increase in the concentration of $W^{5+}O_3^-$ complexes in the studied glasses that act as modifiers [2]. On the other hand, activation energy decrease while the conductivity increases with the increase of WO_3 at the expense of Bi_2O_3 in the glass matrix can be identified by the structural changes in the studied glass system. The frequency exponent, s determined from the slopes of $\ln \sigma$ versus $\ln f$ plots as shown in (Fig. 13(a)), for the present glasses. In the correlated barrier hopping (CBH) model the bipolaron has been proposed to interpret the frequency dependent conductivity. This model was successful in explaining many

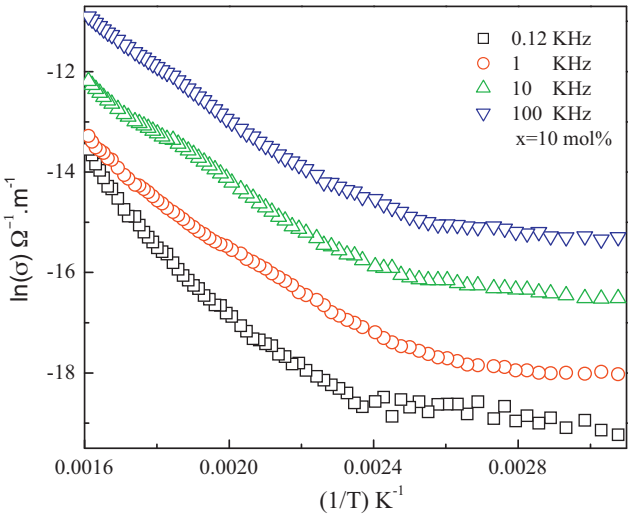

Fig. 12. Plots of $\ln(\sigma)$ versus $1/T$ for $x = 10$ mol%, at different frequencies.

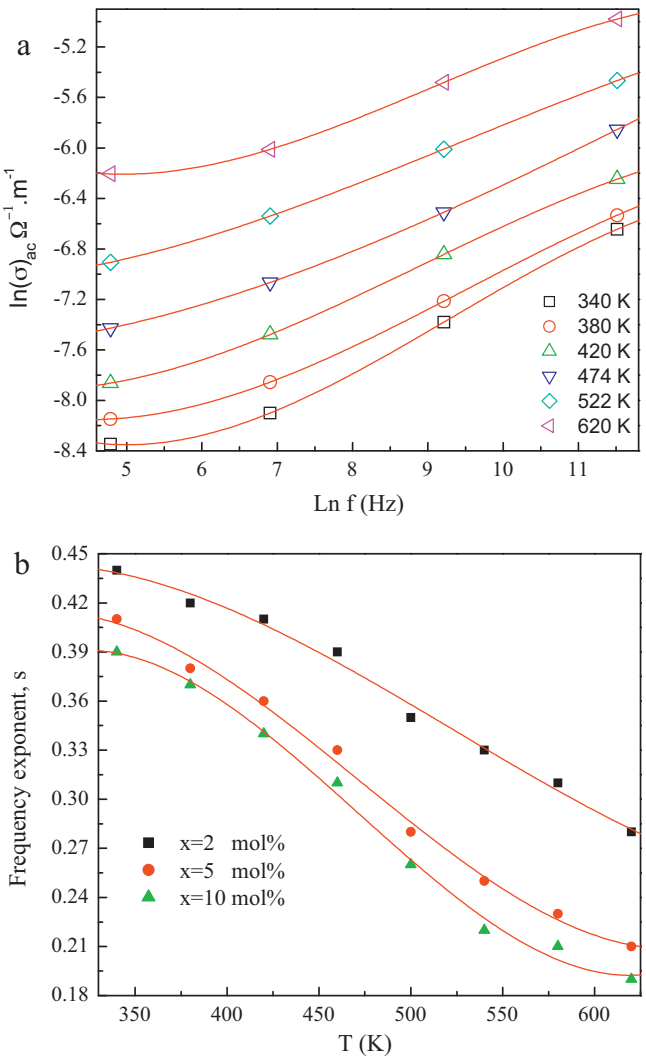

Fig. 13. (a) The plot of $\ln(\sigma_{ac})$ versus $\ln(f)$ for the studied glasses. (b) Temperature dependence of frequency exponent, s, for the studied glasses.

temperature dependent conductivity results at low temperature. However, it does not explain the high temperature behavior particularly in the low frequency range. This theory was extended to high temperature by assuming a single polaron hopping [44], where it produces more satisfactory results. In this respect ac conductivity given for correlated narrow-band limit for random sites and single polaron hopping [40] as:

$$\sigma_{ac}(\omega) = \left(\frac{1}{24}\right)\pi^3\varepsilon_o\varepsilon'\omega\left(\frac{R_\omega}{R}\right)^6 \quad (10)$$

the hopping distance $R_\omega = e^2/\pi\varepsilon_o\varepsilon'[W_M - KT\ln(1/\omega\tau_o)]$, where e is the electronic charge, ε' is the dielectric constant, ε_o is the dielectric constant of free space, W_M is the maximum barrier height, τ_o is the Debye relaxation time [45], and K is the Boltzmann constant. On the contrary, the frequency dependent conductivity in the CBH model can be expressed in terms of the frequency exponent s, by:

$$S = 1 - \frac{6KT}{[W_M - KT\ln(1/\omega\tau_o)]} \quad (11)$$

The CBH model electrons in charged defect states would hop over the coulombic barrier of height W, given as; $W = W_M - [ye^2/\pi\varepsilon_o\varepsilon R]$, where y is the number of electrons to hop $y = 1$ for single polaron case and $y = 2$ for the bipolaron case, and e the electronic charge. Fig. 13(b) displays the temperature dependence of frequency exponent, s, it is noted that s decreases with increase the temperature [2]. This suggests that the correlated barrier hopping conductivity (CBH) is dominant in ac conductivity mechanism of the studied glass system.

4. Conclusions

From the present study of $(65-x)Bi_2O_3$–$15Li_2O$–$20GeO_2$–xWO_3 (where $x = 2$, 5 and 10 mol%) glasses it is observed that the structural units of BiO_6, GeO_6 and WO_6 increase with the increasing of WO_3 content. The changes in density and molar volume with WO_3 content have been discussed in terms of changes in the glass structure. The optical band gap E_g for all types of electronic transitions decreases with increase in WO_3 content due to an increase in the concentration of non-bridging oxygens. The optical energy gap obtained in the case of indirect allowed transition $E_g = 0.86$–1.61 eV which are in good agreement with the estimated values from the imaginary part of dielectric measurements $E_g = 0.85$–1.75 eV. Therefore, the type of electronic transitions in the present glass system is indirect allowed, and the present glasses behave as indirect gap semiconductors. The high values for the refractive index and dispersion are recorded due to the high polarizability of bismuth and tungsten ions. The increase in dielectric constant and loss (ε' and $\tan\delta$) values with increasing WO_3 content could be attributed to charge transfer transition between W^{5+} and W^{6+} ions and that tungsten ions occupy octahedral positions. The DC and AC conductivity increased and activation energies decreased with increase of WO_3 content. Based on these results it is concluded that tungsten ions, enhances the electronic and ionic motion. The temperature dependence of frequency exponent, s, has been explained by correlated barrier hopping model CBH.

Acknowledgement

Authors would like to express their thanks and appreciation to Prof. Dr. M.Y. Hassaan for his distinguished help in the part of electrical measurement.

References

[1] M. Nalin, G. Poirier, S.J.L. Ribeiro, Y. Messaddeq, L. Cescato, J. Non-Cryst. Solids 353 (2007) 1592–1597.
[2] K. Sambasiva Rao, M. Srinivasa Reddy, V. Ravi Kumar, N. Veeraiah, J. Mater. Chem. Phys. 111 (2008) 283–292.
[3] G. Upender, S. Ramesh, M. Prasad, V.G. Sathe, V.C. Mouli, J. Alloys Compd. 504 (2010) 468–474.
[4] P. Subbalakshmi, B.V. Raghavaiah, R. Balaji Rao, N. Veeraiah, Eur. Phys. J. Appl. Phys. 26 (2004) 169.
[5] M. Von Dirke, S. Muller, K. Barner, H. Rager, J. Non-Cryst. Solids 124 (1990) 265.
[6] H. Fan, G. Gao, G. Wang, L. Hu, J. Solid State Sci. 12 (2010) 541–545.
[7] S.M. Salem, E.A. Mohamed, J. Non-Cryst. Solids 357 (2011) 1153–1159.
[8] B.L. Shivachev, T. Petrov, H. Yoneda, R. Titorenkova, B. Mihailova, J. Scripta Mater. 61 (2009) 493–496.
[9] Shashidhar Bale, Syed Rahman, A.M. Awasthi, V. Sathe, J. Alloys Compd. 460 (2008) 699–703.
[10] K. Li, H. Fan, G. Zhang, G. Bai, S. Fan, J. Zhang, L. Hu, J. Alloys Compd. 509 (2011) 3070–3073.
[11] V. Dimitrov, Y. Dimitriev, A. Montenero, J. Non-Cryst. Solids 180 (1994) 51–57.
[12] G.D. Chrysskos, E.I. Kamistos, W.M. Risen, J. Non-Cryst. Solids 93 (1987) 155–168.
[13] X. Jiang, A. Jha, J. Opt. Mater. 33 (2010) 14–18.
[14] S.M. Salem, E.M. Antar, A.G. Mostafa, S.M. Salem, S.A. El-badry, J. Mater. Sci. 46 (2011) 1295–1304.
[15] D. Munoz-Martín, M.A. Villegas, J. Gonzalo, J.M. Fernández-Navarro, J. Eur. Ceram. Soc. 29 (2009) 2903–2913.
[16] G. Upender, S. Suresh Bharadwaj, A.M. Awasthi, V. Chandra Mouli, J. Mater. Chem. Phys. 118 (2009) 298–302.
[17] S.M. Salem, I. Shaltout, J. Mater. Sci. 45 (2010) 1837.
[18] P. Petru, P. Lidia, S. Rada, M. Bosca, E. Culea, Vib. Spectrosc. 48 (2008) 281.
[19] S.G. Motke, S.P. Yawale, S.S. Yawale, J. Bull. Mater. Sci. 25 (1) (2002) 75.
[20] S. Bale, S. Rahman, J. Opt. Mater. 31 (2008) 333.
[21] K. Blaszczak, A. Adamczyk, J. Mol. Struct. 596 (2001) 61.
[22] L. Baia, T. Iliescu, S. Simon, W. Kiefer, J. Mol. Struct. 259 (2001) 9.

[23] P.P. Lottici, I. Manzini, G. Antonioli, G. Gnappi, A. Montenero, J. Non-Cryst. Solids 159 (1993) 173.
[24] G. Little Flower, G. Sahaya Baskaran, N. Krishna Mohan, N. Verraiah, J. Mater. Chem. Phys. 100 (2006) 211.
[25] J. Pankove, Optical Processes in Semiconductors, Prentice-Hall, Englewood Cliffs, NJ, 1971.
[26] J. Tauc, Amorphous and Liquid Semiconductor, Plenum, New York, 1974.
[27] M. Abdel-Baki, F. Abdel-Wahab, A. Radi, F. El-Diasty, J. Phys. Chem. Solids 68 (8) (2007) 1457.
[28] Y. Saddeek, E. Shaaban, E. Moustafa, H. Moustafa, J. Phys. B 403 (2008) 2399.
[29] F. Kremer, J. Non-Cryst. Solids 305 (2002) 1.
[30] S.H. Wample, J. Chem. Phys. 67 (1977) 2151.
[31] M.A. Hassan, C.A. Hogarth, J. Mater. Sci. 23 (1988) 2500.
[32] Y. Yiannopoulos, G. Chryssikos, E. Kamitsos, J. Phys. Chem. Glasses 42 (2001) 164.
[33] K. El-Egili, H. Doweidar, J. Phys. Chem. Glasses 39 (1998) 332.
[34] M.B. Volf, Glass Science and Technology, vol. 7, Elsevier, Amsterdam, 1984, p. 43.
[35] K. Herzfeld, J. Phys. Rev. 29 (1927) 701.
[36] V. Dimitrov, S. Sakka, J. Appl. Phys. 79 (1996) 1741.
[37] T. Sankarappa, M. Prashant Kumar, G.B. Devidas, N. Nagaraja, R. Ramakrishnareddy, J. Mol. Struct. 889 (2008) 308.
[38] E.K. Abdel-Khalek, A.A. Bahgat, Physica B 405 (2010) 1986.
[39] A. Mogus-Milankovic, V. Licina, S.T. Reis, D.E. Day, J. Non-Cryst. Solids 353 (2007) 2659.
[40] S.R. Elliot, J. Adv. Phys. 36 (2) (1987) 135.
[41] M. Shaaban, S.M. Salem, E.M. Antar, E.A. Mohamed, J. Mater. Sci. 46 (2011) 1095–1102.
[42] N.F. Mott, J. Non-Cryst. Solids 1 (1968) 01.
[43] S.M. Salem, J. Alloys Compd. 503 (2010) 242–247.
[44] K. Shimakawa, Philos. Mag. B 46 (1982) 123 (See also p. 48, 77).
[45] N.F. Mott, E.A. Davis, Electronic Processes in Non-Crystalline Materials, 2nd ed., Clarendon Press, Oxford, 1979.